BIOCHEMISTRY
including biophysical chemistry & molecular biology

Article

pubs.acs.org/biochemistry

On the ATP-Dependent Activation of the Radical Enzyme (*R*)-2-Hydroxyisocaproyl-CoA Dehydratase

Stefan H. Knauer,[†,‡,⊥] Wolfgang Buckel,[§,∥] and Holger Dobbek*[,†,‡]

[†]Institut für Biologie, Strukturbiologie/Biochemie, Humboldt-Universität zu Berlin, D-10099 Berlin, Germany

[‡]Bioanorganische Chemie, Universität Bayreuth, D-95440 Bayreuth, Germany

[§]Laboratorium für Mikrobiologie, Fachbereich Biologie, Philipps-Universität, D-35032 Marburg, Germany

[∥]Max-Planck-Institut für Terrestrische Mikrobiologie, D-35043 Marburg, Germany

Supporting Information

ABSTRACT: Members of the 2-hydroxyacyl-CoA dehydratase enzyme family catalyze the β,α-dehydration of various CoA-esters in the fermentation of amino acids by clostridia. Abstraction of the nonacidic β-proton of the 2-hydroxyacyl-CoA compounds is achieved by the reductive generation of ketyl radicals on the substrate, which is initiated by the transfer of an electron at low redox potentials. The highly energetic electron needed on the dehydratase is donated by a [4Fe-4S] cluster containing ATPase, termed activator. We investigated the activator of the 2-hydroxyisocaproyl-CoA dehydratase from *Clostridium difficile*. The activator is a homodimeric protein structurally related to acetate and sugar kinases, Hsc70 and actin, and has a [4Fe-4S] cluster bound in the dimer interface. The crystal structures of the Mg-ADP, Mg-ADPNP, and nucleotide-free states of the reduced activator have been solved at 1.6−3.0 Å resolution, allowing us to define the position of Mg^{2+} and water molecules in the vicinity of the nucleotides and the [4Fe-4S] cluster. The structures reveal redox- and nucleotide dependent changes agreeing with the modulation of the reduction potential of the [4Fe-4S] cluster by conformational changes. We also investigated the propensity of the activator to form a complex with its cognate dehydratase in the presence of Mg-ADP and Mg-ADPNP and together with the structural data present a refined mechanistic scheme for the ATP-dependent electron transfer between activator and dehydratase.

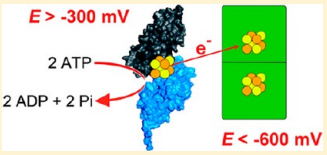

The coupling of ATP hydrolysis to diverse energy-demanding activities in biology is a fundamental but not yet well-understood process in the field of bioenergetics. Nitrogenase[1−4] and protoporphyrinogen reductase,[5−7] several cobalamin containing methyltransferases,[8−10] and the corrinoid iron/sulfur protein (CoFeSP)[11] as well as radical dependent β,α-dehydratases[12−15] and the phylogenetically and mechanistically related benzoyl-CoA reductases[16] rely on ATP-dependent electron transfers (ETs) in which an ATPase harnesses the energy released upon ATP hydrolysis to transfer an electron against the redox potential gradient to their partner proteins. Three groups of ATPases have been shown to act as ATP-dependent electron transferases (ETases) in enzyme systems like nitrogenases, cobalamin-dependent methyltransferases, and β,α-dehydratases.

Nitrogenases catalyze the reduction of dinitrogen to ammonia, for which electrons with very negative reduction potentials are necessary. These electrons are supplied to the dinitrogenase, also called MoFe-protein in the case of the predominant Mo-containing enzyme, by the dinitrogenase reductase, alternatively called Fe-protein (reviewed in refs 1−4). The homodimeric Fe-protein contains a [4Fe-4S] cluster coordinated by two cysteine residues of each monomer.[17,18] Conformational changes associated with ATP-binding, hydrolysis, and release are thought to modulate the potential of the Fe-protein by reorienting the two monomers of the Fe-protein and to trigger association and dissociation of the MoFe-protein/Fe-protein complex.[19,20] Recently, a novel type of ATP-dependent reductive activator has been described, which acts on cobalamin-dependent methyltransferases reducing the inactive Co(II)-state to the active Co(I)-state. This activator contains either a [2Fe-2S] cluster[9−11] or [4Fe-4S] clusters,[8] depending on the cobalamin-containing protein being activated. The biochemical and structural characterization of the activator of CoFeSP, which acts in the reductive acetyl-CoA (Wood−Ljungdahl) pathway, shows that the activator discriminates between the oxidation states of its target protein CoFeSP, ensuring an irreversible electron transfer by only binding to the inactive Co(II)-CoFeSP.[11] Recent work also revealed that this activator, despite very weak sequence similarities, belongs to the ASKHA-fold family (*a*cetate and *s*ugar *k*inases/*H*sc70/*a*ctin), whose members all share the actin fold[21−23] likely inherited from a common ancestor.[23−25] The ASKHA fold has earlier already been detected in the ATP-dependent activator of 2-hydroxyglutaryl-CoA dehydratase from *Acidaminococcus fermentans* (*A. fermentans*),[15,26] indicating a link in the evolution of two of the three types of ATP-dependent ETases. 2-Hydroxy-CoA dehydratases catalyze the atypical dehydration of (*R*)-2-hydroxyacyl-CoA compounds (Scheme 1) for which they rely on the production of ketyl-radical intermediates on the substrate.[12−15] The activators of the different 2-hydroxyacyl-

Received: May 2, 2012
Revised: June 27, 2012
Published: July 24, 2012

   dx.doi.org/10.1021/bi300571z | *Biochemistry* 2012, 51, 6609−6622

Scheme 1. Reactions Catalyzed by 2-Hydroxyacyl-CoA Dehydratases

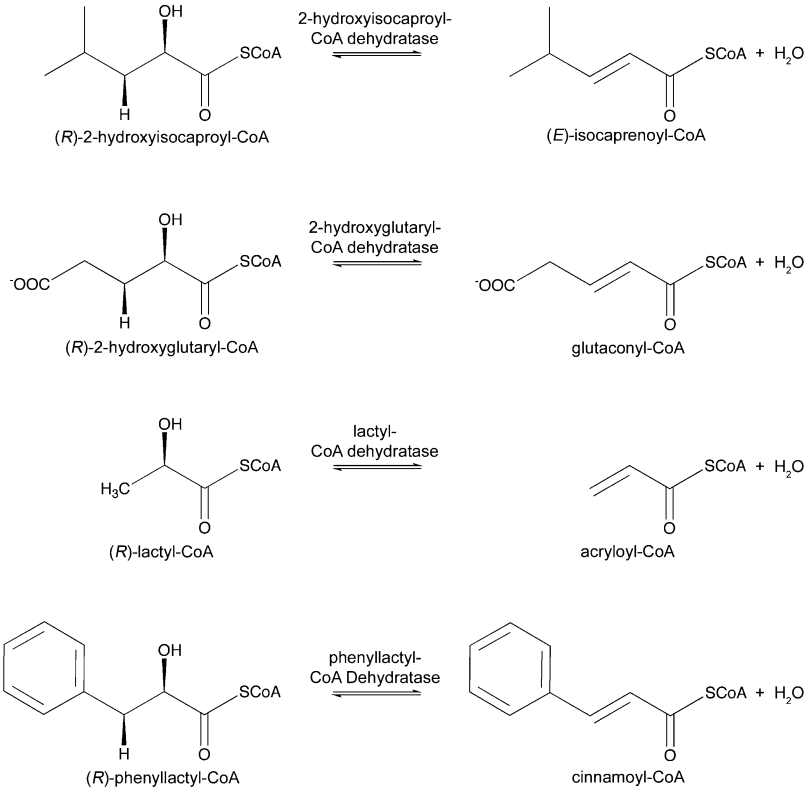

CoA dehydratases are 50−70% identical in their amino acid sequences and are partially functionally exchangeable. Sequences with somewhat lower identities to the activators of the 2-hydroxyacyl-CoA dehydratases are found in many bacterial genomes including nearly all bacteria thriving either strictly or facultatively under anaerobic conditions.[12] These sequences also probably encode ATP-dependent ETases whose targets are different from 2-hydroxyacyl-CoA dehydratases or benzoyl-CoA reductases.

The 2-hydroxyisocaproyl-CoA dehydratase activators exhibit low ATPase activities (0.04 U mg^{-1}), which are 12-fold increased for the oxidized activator in the presence of an excess of 2-hydroxyisocaproyl-CoA dehydratase (0.5 U mg^{-1}) and are the highest when measured for the reduced activator in the presence of 2-hydroxyisocaproyl-CoA dehydratase (2.2 U mg^{-1}).[15] Formation of the activator−dehydratase complex is nucleotide-dependent, and while in the presence of ADP no activator-dehydratase complex can be detected by size exclusion chromatography, ADP-AlF_3 induces a stable complex between the two proteins.[27] The activator can be easily reduced by one electron with sodium dithionite, Ti(III)citrate, or its physiological electron donors, a ferredoxin and a flavodoxin.[28−30] In its $[4Fe\text{-}4S]^+$ state, the cluster can be completely removed by chelating agents like bathophenanthroline disulfonate if ATP is present in the assay but is stable if only ADP is present.[31] As-isolated preparations of the different activators are EPR silent and thus likely in the diamagnetic $[4Fe\text{-}4S]^{2+}$ state but show an $S = 3/2$ signal with $g = 4-6$ after reduction to the $[4Fe\text{-}4S]^+$ state.[30] An all-ferrous ($[4Fe\text{-}4S]^0$) state has been detected for the *A. fermentans* activator in the presence of an excess of Ti(III)citrate, and in this state, it is not able to activate the dehydratase.[32]

The enzyme (*R*)-2-hydroxyisocaproyl-CoA dehydratase catalyzes the *β*,*α*-dehydration of (*R*)-2-hydroxyisocaproyl-CoA (Scheme 1) in the fermentation of L-leucine by *Clostridium difficile* (*C. difficile*).[28] The atypical dehydration depends on the reductive generation of ketyl radicals on the substrate by a single highly energetic electron to yield isocaprenoyl-CoA.[33,34] One electron is transferred from the cognate activator to one of the two [4Fe-4S] clusters of (*R*)-2-hydroxyisocaproyl-CoA dehydratase to activate it and thus to allow up to 10,000 turnovers before the electron is lost in a side reaction and another activation becomes necessary.[28,33,34]

A first insight into how the activation process of 2-hydroxyacyl-CoA dehydratases could proceed was provided by the crystal structure of the activator of (*R*)-2-hydroxyglutaryl-CoA dehydratase from *A. fermentans* (Act_{Af}).[26] The structure of the extremely oxygen-sensitive protein was determined in the ADP-bound, oxidized state and refined at a resolution of 3.0 Å.[26] The homodimer (2 × 27 kDa) was shown to harbor one [4Fe-4S] cluster bridging the two monomers. The fold of the protein identified it as a member of the actin fold family, sharing with other ASKHA members a similar fold and ATP binding site. The structure resolved the position of ADP, but the limited resolution did not allow us to reveal the presence of the Mg^{2+} ion.[26] The key difference between the fold of the activator and that of other members of the ASKHA family were all caused by the presence of the [4Fe-4S] cluster. The cluster is coordinated by four cysteine residues that cause an unusual type of dimerization as it is bound in the dimer interface. It is located at the N-terminus of the *α*-helix 5 from each monomer, which is termed cluster helix. The cluster helices together with the [4Fe-4S] cluster between them enclose an angle of 103°. In analogy to the Fe protein of the nitrogenase system, large conformational changes reorienting

dx.doi.org/10.1021/bi300571z | *Biochemistry* 2012, 51, 6609−6622

the helix-dipoles of the cluster helices were postulated to be one driving force to lower the reduction potential of the [4Fe-4S]$^{2+/+}$ couple.[26,31] The [4Fe-4S] cluster is solvent exposed, which is probably the reason for its high reactivity with dioxygen ($t_{1/2}$ under air ca. 10 s).[12,30,35] The structure of Act_{Af}^{ADP} likely represents the oxidized state of the activator, as no reducing agents were added during purification and crystallization conditions.[26] These conditions have been shown to yield the oxidized activator.[31]

The ATP-dependent activation of 2-hydroxyacyl-CoA dehydratases is only partially understood and still poses many questions as to the role of postulated conformational changes in creating the driving force for the transferred electron and the task of ATP hydrolysis in this context. Especially intriguing is the question whether upon interaction with the dehydratase the angle of 103° between the two cluster helices of the activator widens to 180°,[12,27] similar to that observed with the Fe-protein of nitrogenase with angles of 150° in the free state and almost 180° in the complex with the MoFe-protein stabilized by ADP-AlF_3^-. This movement brings the [4Fe-4S] cluster of the Fe-protein 4 Å closer to the P-cluster of the MoFe-protein and enables electron transfer.[20] Here, we investigated the activator of 2-hydroxyisocaproyl-CoA dehydratase from *C. difficile* (Act_{Cd}) and present its nucleotide-dependent complex formation with 2-hydroxyisocaproyl-CoA dehydratase and crystal structures of the activator in the reduced ADP- and ADPNP-bound, as well as in the nucleotide-free state, at high resolution. Our analysis allows us to further refine the possible mechanism of the ATP-dependent activation of 2-hydroxyacyl-CoA dehydratases.

EXPERIMENTAL PROCEDURES

Anoxic Work. All manipulations were performed under strictly anaerobic conditions in anaerobic glove boxes (Coy Laboratories) under an atmosphere of 95% (g/g) nitrogen and 5% (g/g) hydrogen. Solutions were made anoxic by exchanging the headspace of the bottles and tubes using a vacuum-gas line five times including a minimum of 10 min under low pressure.

Gene Expression and Protein Purification of the Activator. The activator was obtained by overexpression of its gene in *Escherichia coli* (*E. coli*) BL21 CodonPlus(DE3)-RIL as described previously.[28] Purification of the protein with a strep-tag II peptide fused to its C-terminal end was based on published protocols.[26,28] Cells of two or three 5 L-cultures were suspended in 50 mL of buffer (50 mM MOPS (pH 7.2), 0.3 M NaCl, 5 mM EDTA, 2 mM DTT, 1 mM sodium dithionite, and 1 mg/mL lysozyme) and stirred slightly for 30 min. Additionally, either 1 mM ADP or 1 mM ADPNP[36] was added. Subsequently, 1 mg of DNase I, 20 mM $MgCl_2$, and 1% (v/v) Triton X-100 were added, and the solution was incubated for another 30 min. We obtained the crude cell-free extract by ultracentrifugation of the lysate for 70 min at 100,000*g*. The extract was loaded onto a 12 mL StrepTactin Superflow column (IBA GmbH, Germany), which had been equilibrated with 10 column volumes of buffer A (50 mM MOPS (pH 7.2), 0.3 M NaCl, 10 mM $MgCl_2$, 2 mM DTT, and 1 mM sodium dithionite). After loading, the column was washed with 10 column volumes of buffer A before the elution was carried out with two column volumes of buffer B (50 mM MOPS (pH 7.2), 0.3 M NaCl, 10 mM $MgCl_2$, 2 mM DTT, 1 mM sodium dithionite, and 2.5 mM D-desthiobiotin (DTB)) containing either 1 mM ADP or 1 mM ADPNP. Pure protein was concentrated by ultrafiltration (Viva Science, Germany, MWCO 10 kDa) and frozen as well as stored in liquid nitrogen.

Gene Expression and Protein Purification of the Dehydratase. Dehydratase was obtained by overexpression of its genes in *E. coli* BL21 CodonPlus(DE3)-RIL and purified as previously described.[28] Before concentrating by ultrafiltration (Viva Science, Germany, MWCO 30 kDa), the buffer was exchanged to 50 mM MOPS (pH 7.0) containing 2 mM DTT. Finally, dehydratase was shock frozen and stored in liquid nitrogen.

Complex Formation of Activator and Dehydratase. Assays inducing the formation of a complex between activator and dehydratase were based on previously published protocols[27,28] and analyzed by gelfiltration using a HiLoad 16/60 Superdex 200pg column (GE Healthcare, Germany). Two assays for complex formation were investigated, differing in the nucleotide present. Activator and dehydratase were mixed in a molar ratio of 1:1 (10 nmol each) in complex buffer (50 mM MOPS (pH 7.0), 2 mM $MgCl_2$, 5 mM DTT, and 5 mM sodium dithionite) in a final volume of 500 μL. In condition I, ADPNP was added at a final concentration of 1 mM, and an activator purified in the presence of ADPNP was used. In condition II, activator protein was used, which had been purified in the presence of ADP. Here, 2 mM ADP, 100 mM NaF, and 10 mM AlF_3 were added to the complex formation mixture. Stock solutions of NaF (500 mM) and AlF_3 (50 mM) in 50 mM MOPS buffer (pH 7.0) were prepared, mixed in a 1:1 ratio, and centrifuged for 1 min at 12,000*g*, and the supernatant was added to the protein solution.

The complex mixtures were incubated for 60 min, followed by centrifugation for 2 min at 13,000*g*. The supernatant was applied to the gel filtration column equilibrated with gel filtration buffer (50 mM MOPS buffer (pH 7.0), 150 mM NaCl, and 2 mM DTT). This buffer was also used for elution. Gel filtration runs with 1 mg of activator or 1 mg of dehydratase in 500 μL of gelfiltration buffer were performed as references. As a control, a complex formation mixture containing the activator, dehydratase, and 1 mM ADP was prepared, treated like the other complex formation mixtures, and analyzed by gel filtration. For the standard curve, 1 mg of ribonuclease A, 1 mg of ovalbumin, 1 mg of conalbumin, 1 mg of lactate dehydrogenase, and 5 mg of catalase were dissolved in 500 μL of gel filtration buffer.

Oxidation and Reduction of the Activator. To characterize the oxidized and reduced state of the activator, protein that had been purified in the presence of ADP was used. The activator (283 μM) was oxidized by incubation for 30 min in oxidation buffer (50 mM MOPS (pH 7.0), 150 mM NaCl, and 3 mM thionine acetate) in a total volume of 300 μL. The oxidizing agent was removed by buffer exchange against 50 mM MOPS buffer (pH 7.0) containing 150 mM NaCl on a 4-mL Sephadex G25 M column (GE Healthcare, Germany). The protein solution was centrifuged for 1 min at 12,000*g* before being transferred to a 0.5 mL quartz cuvette with 1 cm path length. After blanking against 50 mM MOPS buffer (pH 7.0) containing 150 mM NaCl, we recorded an UV/vis absorption spectrum of oxidized activator at an Agilent 8453 diode array UV−visible spectrophotometer.

For reduction, a 10-fold molar excess of sodium dithionite was added to the oxidized protein solution (final volume 1 mL). After incubation for 30 min, the reducing agent was removed by buffer exchange against 50 mM MOPS buffer (pH 7.0) containing 150 mM NaCl on a 4-mL Sephadex G25 M

dx.doi.org/10.1021/bi300571z | *Biochemistry* 2012, 51, 6609−6622

Table 1. Crystallization Conditions, Data Collection, and Model Refinement Statistics of the Reduced Activator

	crystal 1	crystal 2	crystal 3
		Crystallization	
nucleotide used during purification	ADP	ADPNP	ADP
protein solution	activator (25 mg/mL), 50 mM MOPS (pH 7.2), 0.3 M NaCl, 1 mM ADP, 10 mM $MgCl_2$, 2.5 mM DTB, 2 mM DTT, 10 mM sodium dithionite	activator (21 mg/mL), 50 mM MOPS (pH 7.2), 0.2 M NaCl, 3 mM ADPNP, 7.5 mM $MgCl_2$, 1.9 mM DTB, 1.5 mM DTT, 6 mM sodium dithionite	activator (23 mg/mL), 50 mM MOPS (pH 7.2), 120 mM NaCl, 1.4 mM ADP, 9 mM $MgCl_2$, 1 mM DTB, 6 mM DTT, 1.4 mM sodium dithionite, 100 mM NaF, 10 mM AlF_3
reservoir solution	4 M NH_4acetate, 0.1 M Tris/HCl (pH 8.5)	3.5 M NH_4acetate, 0.1 M Tris/HCl (pH 8.5)	8% (w/v) PEG 8000, 25% (v/v) MPD, 0.35 M NaCl (pH 8.5)
drop setup	2 μL + 2 μL	2 μL + 2 μL	1 μL + 1 μL
cryo solution	3 M NH_4acetate, 0.08 M Tris (pH 8.5), 1 mM sodium dithionite, 20% (v/v) (2*R*,3*R*)-butane-2,3-diol	2.6 M NH_4acetate, 0.08 M Tris (pH 8.5), 1 mM sodium dithionite, 20% (v/v) (2*R*,3*R*)-butane-2,3-diol	7.5% (w/v) PEG 8000, 24% (v/v) MPD, 0.33 M NaCl (pH 8.5), 1 mM sodium dithionite
nucleotide bound	ADP	ADPNP	none
		Data Collection	
wavelength (Å)	0.91841	0.91841	0.91841
space group	*C* 2	*C* 2	$I4_1$
		Unit Cell Parameters	
a/*b*/*c* (Å)	66.2/161.0/63.6	66.1/158.3/63.0	113.1/113.1/56.0
$\alpha/\beta/\gamma$ (°)	90/110.75/90	90/111.97/90	90/90/90
resolution (Å)[a]	30−1.95 (2.00−1.95)	30−1.60 (1.70−1.60)	30−3.0 (3.1−3.0)
unique/observed reflections[a,b]	44,923/169,633 (3,273/12,374)	76,243/222,160 (13,033/37,894)	7,197/52,769 (665/5,040)
redundancy	3.8 (3.8)	2.9 (2.9)	7.3 (7.6)
R_{sym} (%)[a,c]	4.8 (50.1)	5.6 (41.1)	5.9 (48.6)
$I/\sigma I$[a]	16.84 (2.83)	10.27 (2.74)	21.32 (4.35)
completeness (%)[a]	99.4 (99.7)	96.7 (99.5)	99.4 (99.7)
monomers per asymmetric unit	2	2	1
		Refinement Statistics	
R_{work} (%)[d]	17.56	17.14	17.37
R_{free} (%)[e]	20.51	19.67	23.34
		Number of Atoms	
protein	8,071	8,147	1,928
ion/ligand	92	118	4
water	273	535	
		B-Factors	
protein	56.4	38.6	88.5
ion/ligand	39.2	29.9	63.1
water	46.6	42.6	
		rms Deviations	
bond lengths (Å)	0.009	0.008	0.008
bond angles (°)	1.362	1.537	1.107
PDB ID code	4EHT	4EHU	4EIA

[a]Highest-resolution shell values are shown in parentheses. [b]Friedel mates were not treated as independent reflections. [c]$R_{sym} = \Sigma_h\Sigma_i|I_i(h) - \langle I(h)\rangle|/\Sigma_h\Sigma_i I(h)$; where I is the independent observation of reflection h. [d]$R_{work} = \Sigma_h||F_{obs}| - |F_{calc}||/\Sigma_h|F_{obs}|$. [e]The free *R*-factor was calculated from 5% of the data which were removed at random before the structure was refined.

dx.doi.org/10.1021/bi300571z | *Biochemistry* 2012, 51, 6609−6622

column (GE Healthcare, Germany). The eluted protein solution was centrifuged for 1 min at 12,000*g* before being transferred into a 0.5 mL quartz cuvette with 1 cm path length to record an UV/vis absorption spectrum.

Crystallization. The activator was crystallized under reducing conditions in the presence of different nucleotides by vapor diffusion techniques at 16 °C using the hanging-drop setup. Directly before setting up the drops, the protein was incubated with 5−10 mM sodium dithionite and the nucleotide (10 min for ADP and ADPNP, 1 h for ADP-AlF_3) and then centrifuged for 1 min at 12,000*g*. The composition of the protein and reservoir solutions is shown in Table 1.

An activator purified in the presence of ADP was crystallized in the presence of ADP (crystal 1) and in the presence of ADP and AlF_4^- (crystal 3). For crystallization with ADP-AlF_3, solutions of 500 mM NaF and 50 mM AlF_3 in 50 mM MOPS buffer (pH 7.2) were prepared. These stock solutions were mixed in a 1:1 ratio and centrifuged for 1 min at 12,000*g* before the supernatant was added to the protein solution. After incubation for 1 h, the protein solution was concentrated by ultrafiltration (VivaScience, Germany, MWCO 10 kDa). Protein purified in the presence of ADPNP was used to crystallize the activator in the presence of this ATP analogue (crystal 2). Crystallization conditions are summarized in Table 1.

Crystals were harvested and cryo-cooled at the latest 48 h after setting up crystallization drops under anoxic conditions in a glovebox. For storage, crystals were transferred to a cryo solution (see Table 1) in which they remained for a few seconds before they were cooled and stored in liquid nitrogen.

Determination of the Oxidation State of Crystallized Activator. UV/vis spectra from eight dissolved activator crystals, which had been crystallized in the presence of ADP, were recorded to determine the oxidation state of the [4Fe-4S] cluster. First, the cryo-cooled crystals were thawed in a glovebox. Then, each single crystal was washed twice in fresh drops containing 5 μL of MOPS buffer (pH 7.0) before all crystals were dissolved in a new drop containing 8 μL of MOPS buffer (pH 7.0). UV/vis absorption spectra of the protein solution were recorded on a Nanodrop spectrometer (PEQLAB) and averaged.

Data Collection, Structure Determination, and Structure Analysis. Diffraction data were collected at the synchrotron beamlines 14.1 and 14.2 (BESSY, Berlin, Germany). The crystal was cryocooled in a stream of nitrogen at 100 K. Data were processed and scaled with XDS.[37] To obtain initial phases for crystals 1 and 2, Patterson search techniques with the homologous search model were performed using PHASER.[38] One monomer of the activator of the (*R*)-2-hydroxyglutaryl-CoA dehydratase from *A. fermentans* (PDB ID: 1HUX)[26] was used as the search model. In both cases, the resulting electron density was of good quality so that a first model could be built using RESOLVE.[39] Subsequent rounds of model building and refinement were performed using the programs COOT[40] and PHENIX.[41] Each monomer was treated as a TLS group, and riding hydrogens were incorporated in the model for refinement.

The Patterson search technique with a homologous search model with PHASER[38] was also used for phasing of crystal 3. Here, the separated domains I and II of a monomer of the activator with ADP (crystal 1) served as search models, while the C-terminal helix was added to domain I. Domain I comprised amino acids 1−94 and 243−260, and domain II contained amino acids 95−242. To minimize the model bias, a refinement cycle including a simulated annealing energy minimization using PHENIX[41] was performed. Subsequent rounds of model building and refinement were performed using the programs COOT[40] and PHENIX.[41]

Data collection and refinement statistics are shown in Table 1. All figures were generated using PyMOL.[42] Structure superimpositions were performed with COOT[40] or LSQMAN.[43] Channels were calculated using HOLLOW,[44] and angles between α-helices were calculated with MOLMOL.[45]

Coordinates and structure factor amplitudes are deposited in the Protein Data Bank (PDB) with ID codes 4EHT (activator in complex with ADP), 4EHU (activator in complex with ADPNP), and 4EIA (nucleotide-free state of activator).

RESULTS

Nucleotide-Dependent Complex Formation. Complex formation between the activator and dehydratase was investigated by size exclusion chromatography (Figure 1). The elution volumes of dehydratase and activator alone

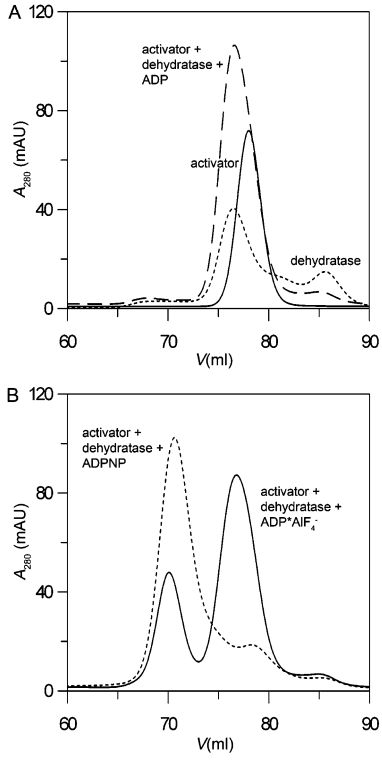

Figure 1. Complex formation between activator and dehydratase. Complex formation was investigated by gel filtration. In A, the chromatograms of activator alone (—, 1 mg), dehydratase alone (·····, 1 mg) and activator + dehydratase + ADP (-----) are shown; in B, the chromatograms of activator + dehydratase + ADPNP (·····) and activator + dehydratase + ADP + AlF_4^- (—) are depicted. The mixtures for complex formation contained the activator and dehydratase (50−100 μM each) in a molar ratio of 1:1 in 50 mM MOPS buffer (pH 7.0), 2 mM $MgCl_2$, 5 mM sodium dithionite, and 5 mM DTT with a final volume of 500 μL. Additionally, 2 mM ADP or 2 mM ADP, 100 mM NaF, and 10 mM AlF_3 or 1 mM ADPNP was added. The complex mixtures were incubated for 1 h before they were applied to the gel filtration column. MOPS buffer (50 mM, pH 7.0) containing 150 mM NaCl and 2 mM DTT was used as the running buffer.

dx.doi.org/10.1021/bi300571z | *Biochemistry* 2012, 51, 6609−6622

corresponded to molecular masses of 82 kDa and 72 kDa, respectively (calculated molecular mass of the dehydratase, 89.9 kDa, and of the activator, 59.2 kDa[46]) (Figure 1A). In addition to a peak corresponding to the physiological heterodimeric dehydratase component, a peak at larger volumes was detected that likely corresponds to an isolated subunit of the dehydratase. The elution behavior of the activator remained the same and was independent of the presence of ADP or ADPNP during purification or incubation with ADP and AlF_4^- before the run. The mixture of dehydratase with activator and ADP from *C. difficile* (Act_{Cd}^{ADP}) led to a single elution peak, resulting from the overlap of the elution peaks of Act_{Cd}^{ADP} and dehydratase (Figure 1A). In contrast, when ADPNP or ADP and AlF_4^- were present in the mixture, an additional elution peak corresponding to a molecular mass of 131 kDa appeared (Figure 1B). An analysis of the fractions of this additional peak by SDS−PAGE showed that both Act_{Cd} and dehydratase were present in the eluted fractions. Hence, we conclude that the presence of the ATP analogue ADPNP and the transition state analogue ADP-AlF_3 induced complex formation between the activator and dehydratase (theoretical molecular mass of the complex: 149 kDa[46]).

Oxidation State of Act_{Cd}^{ADP}. To determine the oxidation state of the activator in the crystal, cooled crystals of Act_{Cd}^{ADP} were dissolved, and a UV/vis absorption spectrum was recorded. The resulting spectrum resembles the spectrum of the reduced activator (Figure 2). All crystals were harvested and

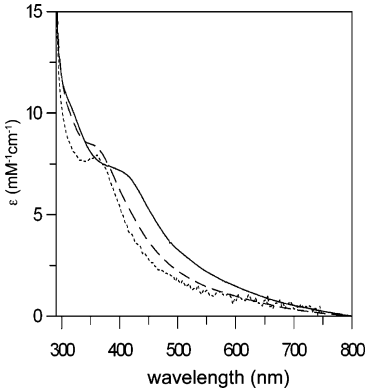

Figure 2. Redox state of Act_{Cd}^{ADP}. UV/vis spectra of oxidized (——) and reduced activator (-----). The oxidation was carried out with a 10-fold molar excess of thionin acetate, the reduction with a 10-fold molar excess of sodium dithionite in 50 mM MOPS buffer (pH 7.2) containing 150 mM NaCl. The reducing or oxidizing agent was removed by buffer exchange with a sephadex G25-column. Crystals of Act_{Cd}^{ADP} were thawed, washed, and dissolved in 50 mM MOPS buffer (pH 7.0). The UV/vis absorption spectrum of the resulting protein solution is shown (·····).

frozen in liquid nitrogen no later than 48 h after setting up crystallization drops in the presence of the reducing agent sodium dithionite. Hence, we conclude that the structure of Act_{Cd}^{ADP} represents the reduced state of the protein. Crystallization experiments as well as harvesting and freezing of the crystals of the activator in the presence of ADPNP and ADP-AlF_3 were conducted as described for Act_{Cd}^{ADP}. Presuming that nucleotide binding to the activator has no strong influence on the reduction potential of the $[4Fe\text{-}4S]^{2+/+}$ couple, we conclude that the activator was always reduced so that the resulting structures represent the reduced state.

Overall Structure of Act_{Cd}^{ADP}. We crystallized the recombinant activator under anoxic and reducing conditions in the presence of ADP. Patterson search techniques with a homologous search model were used to obtain initial phases in which the activator of the (*R*)-2-hydroxyglutaryl-CoA dehydratase from *A. fermentans* (PDB code: 1HUX)[26] served as the search model. Two monomers connected by a 2-fold rotation axis forming the native dimer were found in the asymmetric unit. The structure was refined to a resolution of 1.95 Å and revealed that each monomer harbors a nucleotide-binding site in which ADP is located with full occupancy (Figures 3A−C). The monomers are nearly identical with an rms deviation of 0.49 Å for the corresponding C_α atoms. The functionally important [4Fe-4S] cluster is positioned at the dimer interface and bridges the monomers.

Each monomer harbors two domains, which are arranged to give an "L" shaped architecture (Figure 3C), and domain II can be further divided into subdomains IIa and IIb (Figure S1, Supporting Information). Each monomer exhibits a mixed α/β topology with 8 α-helices and 10 β-strands, where the latter are arranged in 2 five-stranded β-sheets. The β-sheets are located in domains I and IIa and enclose an angle of ca. 60°. Two α-helices (h2 and h8, Figure S1, Supporting Information), nearly perpendicular to each other, are positioned in the cleft between the β-sheets. The nucleotide-binding site is at the interface of domains I and II positioning the β-phosphate at a distance of 17 Å from the [4Fe-4S] cluster (Figure 3C). On the basis of its topology, the activator belongs to the ASKHA fold family.[21−23] The ASKHA fold comprises two nearly symmetric domains with $\beta\beta\beta\alpha\beta\alpha\beta\alpha$ topology forming the core of the proteins. Connecting loops are variable, and additional domains can be inserted into the loop regions, facilitating the individual functions of the enzymes.[21−23] Domains I and IIa of Act_{Cd}^{ADP} exhibit this typical topology with domain IIb being an α-helical bundle which is inserted into domain IIa.

Act_{Cd} and Act_{Af}[26] share a sequence identity of 54%, and consequently, their crystal structures, which were both determined in the presence of ADP, are very similar and can be superimposed with an rms deviation (rmsd) for C_α-atoms of 1.2 Å. The structure of Act_{Af} with bound ADP (Act_{Af}^{ADP}) likely represents the oxidized state of the activator. In contrast, the structure of Act_{Cd}^{ADP} has been determined from a reduced enzyme preparation, crystallized in the presence of the reducing agent sodium dithionite. This indicates that the oxidation state of the [4Fe-4S] cluster does not affect the overall conformation of the activator.

ADP Binding. ADP is noncovalently bound at the close edges of the β-sheets with the phosphate groups positioned in an 8 Å long tunnel (Figure 3C). The amino acids interacting with ADP are shown in Figures 4A and S2A (Supporting Information). The β-phosphate of ADP interacts with Nε of Lys14, which is also in hydrogen bonding distance to the α-phosphate. An additional interaction partner of the β-phosphate was modeled as a Mg^{2+} ion. The Mg^{2+} ion could not be identified in the structure of Act_{Af}^{ADP}, due to the limited resolution.[26] We identified the Mg^{2+} ion in the structure of Act_{Cd}^{ADP} based on its typical octahedral coordination, here by the β-phosphate and five water molecules with an average distance of 2.2 Å. These distances are in the range of the average Mg^{2+}−oxygen distance of 2.08 Å known from small molecule structures with octahedral coordinated Mg^{2+} ions.[47] The interpretation also satisfies the electron density maps after refinement. Furthermore, $MgCl_2$ was present in the crystal-

dx.doi.org/10.1021/bi300571z | *Biochemistry* 2012, 51, 6609−6622

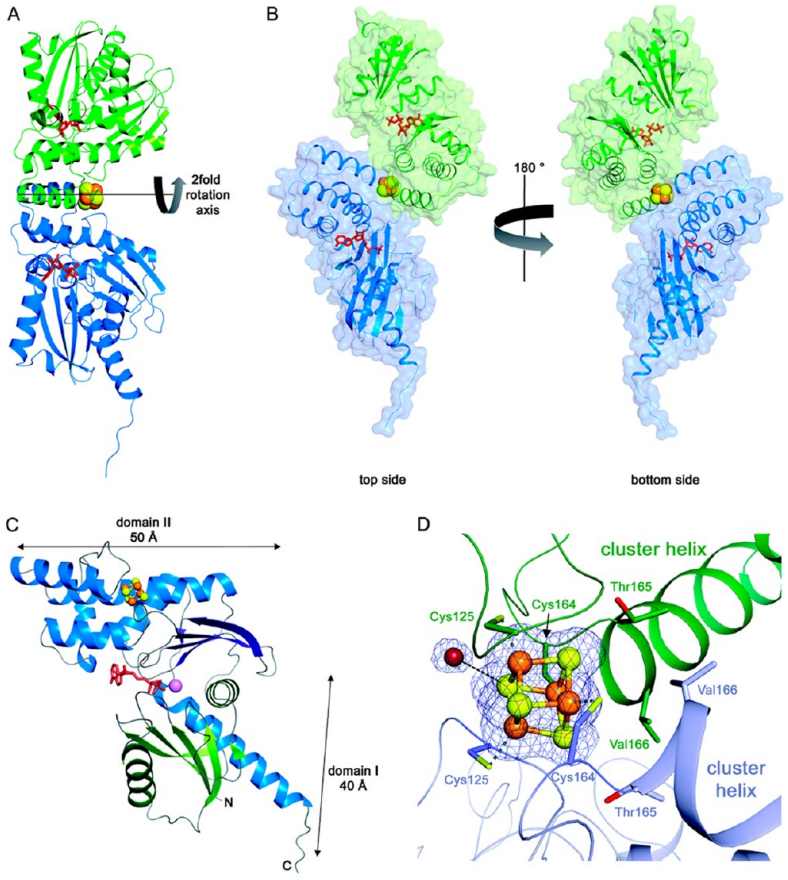

Figure 3. Structure of the activator with bound ADP. (A) The monomers are displayed in ribbon representation in blue and green. Additionally, the surface representation is shown in B. The [4Fe-4S] cluster is depicted as spheres with iron atoms in orange and sulfur atoms in yellow, ADP is shown as red sticks. (C) Topology of one monomer. α-Helices and β-sheets of domain I are colored in dark and bright green, respectively, α-helices and β-sheets of domain II are colored in bright and dark blue, respectively. Loops are shown in gray. The Fe/S cluster is depicted as balls and sticks, ADP as sticks (colors as described in A), and Mg^{2+} as violet spheres. (D) Coordination of the bridging [4Fe-4S] cluster. The Fe/S cluster is shown as in B. Monomers are shown in ribbon representation in green and blue. Selected amino acids are shown as sticks with carbon atoms in the colors of the corresponding monomers, oxygen atoms in red, and sulfur atoms in yellow. The water molecule is represented as a red sphere. The simulated annealing omit map contoured at 3 σ is shown in dark blue. Hydrogen bonds and coordinating bonds are shown as dashed lines in gray and black, respectively.

lization condition. The Mg^{2+} ion is only indirectly coordinated by the protein matrix, which forms the second coordination sphere by interacting with the Mg^{2+} coordinating water molecules with four side chains (Asp7, Glu79, His83, and Asp99), of which Asp7 and Asp99 act as bidentate ligands (Figure 4A). The β-phosphate is connected to the [4Fe-4S] cluster via two loops (amino acids 102−105 and 122−128) (Figure S3, Supporting Information). The second loop harbors Cys125, which is a ligand of the [4Fe-4S] cluster.

Environment of the [4Fe-4S] Cluster. The bridging [4Fe-4S] cluster is coordinated by four cysteine residues, two from each monomer (Cys125 and Cys164, Figure 3D). Weak hydrogen bonds between the amide NH-group of Thr165, the hydroxy group of Thr165, and the two nonsolvent exposed sulfido ligands of the [4Fe-4S] cluster are indicated by a distance of 3.4−3.5 Å between possible H-bond donor and acceptor atoms. The cluster is positioned at the N-terminal end of an α-helix in domain II, which has been termed cluster helix[26] (Figure 3D), directly on the extension of the helix axis. Together with the cluster helices, the [4Fe-4S] cluster forms the central unit of the dimer. The helices enclose an angle of 95.6°, the so-called helix−cluster−helix angle, which is similar to the 103° found in Act_{Af}^{ADP}.[26]

Residues Thr165 and Val166 are located at the N-terminal end of the cluster helix and form a rectangle in the dimer that shields the [4Fe-4S] cluster from the solvent on this side (top side) (Figure 3B and D). The opposite side of the cluster (bottom side) is solvent-accessible, and a water molecule is found in hydrogen bonding distance to one of the sulfur atoms (Figure 3D). The side chain of Arg196 adopted two conformations in the structure (R196a and b in Figure 5A). In the dominant conformation (labeled R196a), Arg196 is in an extended conformation and positions the guanidinium group closely to the thiolate group of Cys125 (Nω (R196)−Sγ (Cys125): 3.6 Å). As this interaction is the same in both monomers, two positive charges are in close proximity to the [4Fe-4S] cluster and stabilize the negative charge of Cys125 on both monomers, effectively reducing the reduction potential of the [4Fe-4S] cluster. The Arg196 pair together with Lys124 and Arg203 creates a distinctively positively charged patch

dx.doi.org/10.1021/bi300571z | *Biochemistry* 2012, 51, 6609−6622

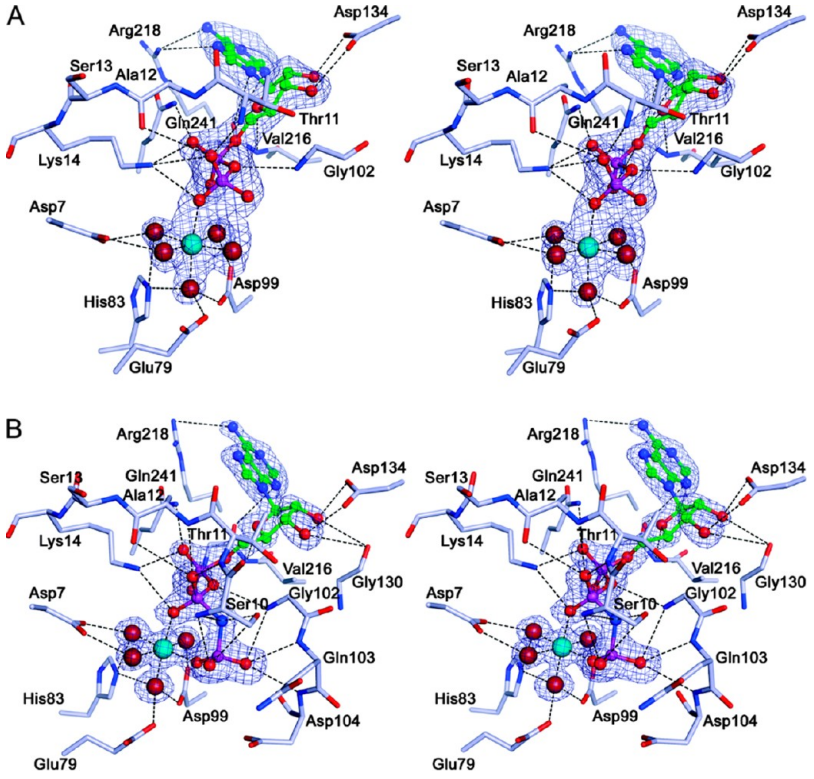

Figure 4. Nucleotide-binding site. Stereoview of the ATP binding site with (A) ADP and (B) ADPNP. Nucleotides are represented as balls and sticks, interacting residues as sticks with oxygen atoms colored in red, nitrogen atoms in blue, phosphorus atoms in purple, carbon atoms of amino acids in gray, and carbon atoms of nucleotides in green. Water molecules and Mg^{2+} ions are depicted as red and cyan spheres, respectively. Hydrogen bonds are shown as dashed lines in black. The simulated annealing omit map contoured at 3 σ is shown in dark blue.

around the [4Fe-4S] cluster at the surface of Act_{Cd} (Figure 5C). The equivalent residue in the oxidized structure of Act_{Af}^{ADP}, Arg198, (Figure 5B) is in a different conformation, equivalent to the second conformation observed for Arg196 (R196b, Figure 5A) moving the guanidinium group away from the [4Fe-4S] cluster (Nω (R198)−Sγ (Cys127): 8.7 Å). The solvent exposure of the [4Fe-4S] cluster is similar in Act_{Cd}^{ADP} and Act_{Af}^{ADP}.

Binding of ADPNP. Cocrystallization of the activator with the ATP analogue ADPNP under reducing conditions resulted in crystals belonging to the same space group and with similar unit cell constants as the crystals of Act_{Cd}^{ADP} (Table 1). Again, one dimer was found per asymmetric unit. The structure was refined to 1.6 Å resolution. The overall structure as well as the topology of the monomers are identical to Act_{Cd}^{ADP}, and accordingly, both dimers can be superimposed with an rmsd value for C_α-atoms of 0.4 Å. In each nucleotide binding site, one molecule ADPNP is noncovalently bound, with its ADP moiety forming nearly the same interactions as those found for ADP in Act_{Cd}^{ADP} (Figures 4 and S2, Supporting Information). A minor difference is found in the interactions of the protein with the vicinal hydroxy groups of the ribose, which in Act_{Cd}^{ADPNP} are not only coordinated by Asp134 but also by the carbonyl oxygen of Gly130. The phosphate groups are positioned in the tunnel with the γ-phosphate at the open side allowing dissociation of P_i after ATP hydrolysis. The presence of the γ-phosphate group causes some small changes in comparison to the Act_{Cd}^{ADP} structure. A loop comprising amino acids 9−12 moves toward the γ-phosphate and brings the hydroxy group of Ser10 in hydrogen-bonding distance to the imido group between the β- and γ-phosphates and an oxygen atom of the γ-phosphate (Figures 4B, S3 and S4 (Supporting Information)). The γ-phosphate interacts with the hydroxy group of Ser10 as well as the main chain atoms of Gly102, Gln103, and Asp104. As in the structure of Act_{Cd}^{ADP}, a Mg^{2+} ion is found in the nucleotide binding site, which is octahedrally coordinated by the β- and γ-phosphate and four water molecules with an average distance of 2.1 Å. Several water molecules are found near the γ-phosphate; however, none of them is correctly placed to act as the attacking nucleophile in an *in-line* nucleophilic substitution mechanism. The environment of the [4Fe-4S] cluster is the same as in Act_{Cd}^{ADP} with a slightly larger helix−cluster−helix angle of 98.7°. Arg196 is again in the elongated conformation with the short distance between the guanidinium group and Cys125. The shortest distance of the β- and γ-phosphate to the Fe/S cluster is 17 Å and 15.5 Å, respectively.

Structure of the Nucleotide-Free State. The activator was also crystallized under reducing conditions in the presence of ADP and AlF_4^-. The resulting crystals belong to space group $I4_1$, and only one monomer was found per asymmetric unit (Table 1). The crystallographic symmetry creates the native dimer with the [4Fe-4S] cluster bridging the monomers (Figure 6A). In the structure (3.0 Å resolution), the topology of a monomer is the same as in Act_{Cd}^{ADP}, but the angle between domains I and II is increased by approximately 40°. Although ADP and AlF_4^- were present during crystallization experiments, the nucleotide-binding site was empty so that this structure represents the nucleotide-free state (Act_{Cd}^{empty}). A superimposition with Act_{Cd}^{ADP} demonstrates that the central part of the dimer comprising the [4Fe-4S] cluster and the domains II remains rigid, while domain I moves outward pivoting around

dx.doi.org/10.1021/bi300571z | *Biochemistry* 2012, 51, 6609−6622

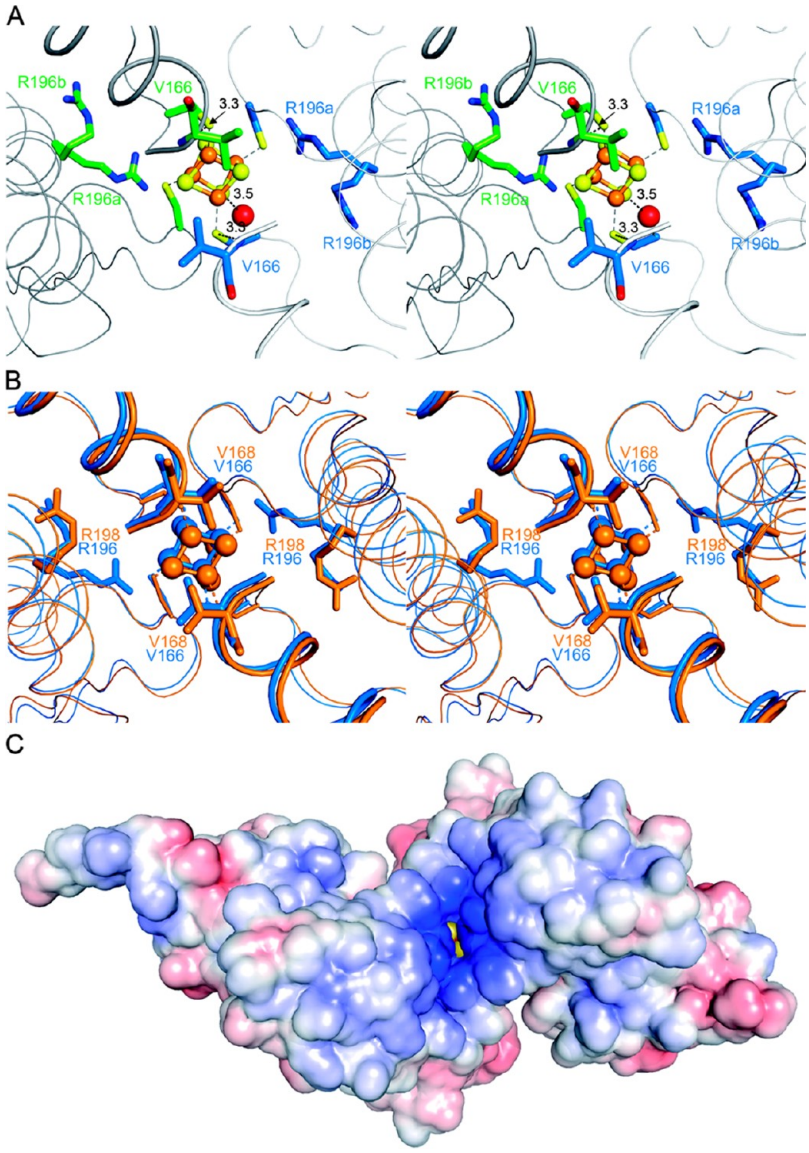

Figure 5. Environment around the [4Fe-4S] cluster. (A) Stereoview of the [4Fe-4S] cluster environment. Carbon atoms of side chains have been colored light blue or green to distinguish the two monomers coordinating the [4Fe-4S] cluster. (B) Stereoview of the superimposition between the reduced Act_{Cd}^{ADP} (blue) and oxidized Act_{Af}^{ADP} (PDB ID: 1HUX). (C) Electrostatic surface potential presentation mapped onto the solvent accessible surface of Act_{Cd}^{ADP}. Coloring from blue (+5 kT) to red (−5 kT). Only the partial charges of the protein, excluding the [4Fe-4S] cluster have been used for the electrostatic potential calculation using PDB2PQR[61,62] and APBS2[63] implemented in PyMol.[42] The [4Fe-4S] cluster is shown as spheres and is partially visible in the middle of the positively charged spot in the center of the protein.

helix 2, which acts as a hinge (Figure 6B). The movement shifts helix 1 by approximately 19 Å. The position as well as the coordination of the [4Fe-4S] cluster is the same as in Act_{Cd}^{ADP}. The helix−cluster−helix angle is 104.6°.

Cycling between a nucleotide-bound, closed state and a nucleotide-free, open state appears to be an abundant motif for members of the ASKHA fold family. While most structures feature the closed conformation, an open conformation of a nucleotide-free enzyme, not unlike Act_{Cd}^{empty}, has been observed for DnaK, when bound to the nucleotide exchange factor GrpE[48] and hexokinase,[49,50] as well as for Arp2 and Arp3.[51]

DISCUSSION

The mechanism of the ATP-dependent activation of 2-hydroxyacyl-CoA dehydratases is only partially understood. While it appears obvious that the energy derived from ATP hydrolysis is used to drive electron transfer, the mechanistic base for this conversion is unclear, and several different mechanistic pathways appear possible (Figure 7). Two pertinent questions are as follows: (A) how is the reduction potential of the $[4Fe\text{-}4S]^{2+/+}$ couple of the activator lowered to be able to transfer an electron to the low potential [4Fe-4S] cluster ($E_m' < -600$ mV) of the dehydratase,[28] and (B) what is the role of ATP hydrolysis in this process?

Driving Force for the Electron Transfer. Conformational changes modulating the reduction potential of the [4Fe-4S] cluster are likely driving the electron transfer between the activator and the dehydratase. The conformational changes could have been dependent on the type of nucleotide (ADP vs. ATP) bound to the activator. However, our crystallographic analysis revealed only little structural differences between the

dx.doi.org/10.1021/bi300571z | Biochemistry 2012, 51, 6609−6622

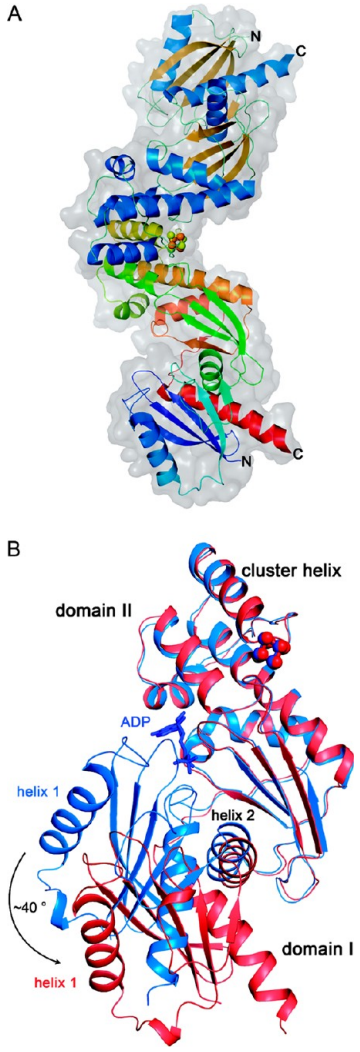

Figure 6. Structure of Act_{Cd}^{empty}. (A) Ribbon and surface representation of the Act_{Cd}^{empty} dimer. The upper monomer is colored according to secondary structure with α-helices in blue, β-sheets in dark yellow, and loops in green. The lower monomer is colored in rainbow colors from the N-terminus in blue to the C-terminus in red. The [4Fe-4S] cluster is shown as balls and sticks (sulfur atoms in yellow and iron atoms in orange). (B) Superimposition of monomers of Act_{Cd}^{ADP} (blue) and Act_{Cd}^{empty} (red) based on C_α atoms of domain II. The monomers are shown in ribbon representation; ADP is displayed as sticks, and the Fe/S clusters as balls and sticks.

two states and showed a practically identical environment for the [4Fe-4S] cluster in the presence of ADP and ADPNP, as well as in the absence of any nucleotide. Our structural analysis does not necessarily reflect the different conformations, which may be adapted by the activator in solution. The nucleotide-dependent formation of the activator–dehydratase complex already indicates that ADP- and ATP(ADPNP)-bound Act_{Cd} act more differently than anticipated based on the structure alone. This can be explained by different scenarios: (A) the activator always adopts an ensemble of different conformations in solution, whose populations may be dependent on the nucleotide bound and which are in a dynamic equilibrium. From this "conformational sampling" hypothesis[52] for the activator, we would reason that the crystallization conditions we chose selected the same "crystallizable" conformation from the ensemble present with the two nucleotides, whereas formation of the complex with the dehydratase selects another conformation, which is only appreciably populated in Act_{Cd}^{ATP}. (B) Alternatively, both Act_{Cd}^{ADP} and Act_{Cd}^{ATP} could not only adopt the same conformation in the crystal but also in solution, and both are able to form a weak encounter complex with the dehydratase. However, only Act_{Cd}^{ATP} may progress toward the formation of a stable complex, as this needs a conformational change induced by contact with the dehydratase, which is only stabilized when ATP is bound to the activator. Clearly, we cannot distinguish between the two hypotheses at the current time, and other explanations are possible. The phenomenon that a crystallographic analysis does not reflect the conformational flexibility in solution is also known from other members of the ASKHA family.[53−55]

In contrast, local conformational changes are uncovered by our structure in which the conformation of Arg196 appears to depend on the oxidation state of the [4Fe-4S] cluster (Figure 5B). Moving two positive charges upon reduction about 5 Å toward the [4Fe-4S] cluster would strongly stabilize the reduced state and thus facilitate the reduction of the [4Fe-4S] cluster of the activator during turnover. The conformation of Arg196 may additionally be altered upon complex formation with the dehydratase. The two [4Fe-4S] clusters of the dehydratase are buried in the protein, and only an electron donor placed near the protein surface will be able to transfer an electron directly to one of the [4Fe-4S] clusters.[34] To be within direct ET distance,[56] the activator would have to bind with its bottom-side (Figure 3A) to the dehydratase. Protein–protein interactions frequently involve conformational changes of side chains in the contact area, and in case of the dehydratase–activator complex, Arg196 will likely be part of the contact area. Furthermore, protein–protein interactions typically lead to a desolvation of the contact areas.[57] Our structural analysis clearly showed that the [4Fe-4S] cluster is solvent exposed and forms hydrogen bonds to localized water molecules on the surface of the protein. Hydrogen bonds are one of the key factors in the modulation of the reduction potential of Fe/S cluster.[58] The desolvation/dehydration of [4Fe-4S] clusters strongly increases their reduction potential.[57] Thus, complex formation alone may be able to shift the reduction potential of the $[4Fe\text{-}4S]^{2+/+}$ couple. In the case of the dehydratase–activator complex, the contact area between both proteins would likely include the solvent exposed side of the [4Fe-4S] cluster and would revoke its solvent exposure. Removing the water molecules from the [4Fe-4S] cluster of the activator would make its environment similar to the β-cluster of the dehydratase, which is completely shielded from the solvent and may be able to match the $[4Fe\text{-}4S]^{2+/+}$ reduction potentials of both [4Fe-4S] clusters.[34] A change of solvent exposure of a [4Fe-4S] cluster upon protein–protein complex formation has already been suggested as a major tuner of the reduction potential and shifts of at least −300 mV are possible.[57]

In summary, all three factors, overall conformational changes, and the redox-dependent movement of Arg196 as well as desolvation may add up to achieve the necessary increase in the reducing power in the activator. As they all depend on complex formation, they could at the same time ascertain the specificity of ET.

Role of ATP hydrolysis. What may be the role for ATP hydrolysis in this process? The rate of ATP hydrolysis by the activator is relatively low and is stimulated up to 55-fold in the presence of its cognate dehydratase.[15,28] In light of the above discussion, we can now better understand the stimulation as we

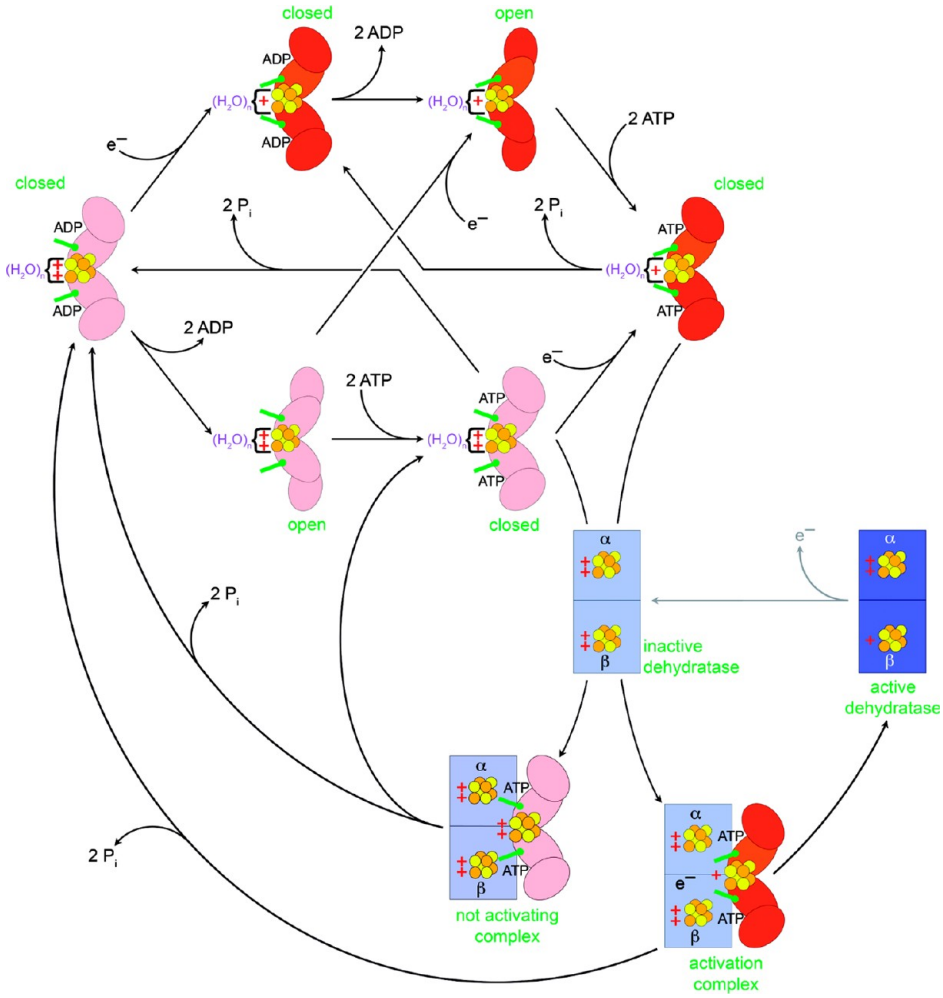

Figure 7. Reaction network of 2-hydroxyacyl-CoA dehydratase activators. Arrows indicate the different electron transfers and binding steps possible for the reaction of 2-hydroxyacyl-CoA dehydratase activators. "Closed" denotes the activator conformation observed in the presence of ADP and ADPNP and "open" the conformation without the nucleotide bound. The charge of the [4Fe-4S] cluster core is indicated by cross symbols and emphasized by the color of the protein with dark shades denoting the reduced state. Two green sticks represent the redox-dependent conformation of Arg196.

revealed that Act_{Cd}^{ATP} forms a complex with the dehydratase, which, if it invokes a new conformation on Act_{Cd}^{ATP}, may increase the rate of ATP hydrolysis. This is even more likely as it has been shown that the activator also forms a stable complex with the dehydratase in the presence of the transition state analogue ADP-AlF_3 (Figure 1),[27] and it thus appears probable that the ATP-containing activator when bound to the dehydratase has the same or a similar conformation as that of the ADP-AlF_3 containing activator bound to the dehydratase. Parts of the binding energy from complex formation may thus be used to stabilize the conformation adopted by the activator in the transition state of ATP-hydrolysis, which would lower the activation barrier for hydrolysis. The assumption of a conformational change of Act_{Cd}^{ATP} when it forms the complex would explain the stimulation of its ATPase activity, as well as the reason why we observed similar conformations for Act_{Cd}^{ADP} and Act_{Cd}^{ADPNP}, because both are in the conformation with low ATPase activity, and it needs complex formation with the dehydratase to bring Act_{Cd}^{ATP} into the conformation with high ATPase activity. The absence of a good candidate for the attacking nucleophile in an *in-line* mechanism supports the notion that the crystal structure of Act_{Cd}^{ADPNP} represents a state of low ATPase activity.

Within this context, it should be noted that Act_{Cd}^{ADP} does not form a complex with the dehydratase (Figures 1 and 7).[27] This is important for two reasons: (A) to receive an electron from its physiological electron donors,[29,59] the [4Fe-4S] cluster of the activator needs to be accessible or at least be in ET distance to the partner and should not be covered by the bulky dehydratase. (B) Once activated, the dehydratase needs to keep its low-potential electron and hide it from side reactions. If Act_{Cd}^{ADP} would remain bound or would easily rebind to the dehydratase ET would become reversible resulting in ET from the dehydratase to the ADP-bound activator, which would waste ATP. Given the low yield of ATP in the fermentation of isoleucine, the irreversibility of ET between activator and dehydratase appears mandatory in this system.[60]

Finally, ATP-hydrolysis may not be necessary for ET between the activator and dehydratase. The different propensities of the ATP- versus ADP-bound activator to form a complex with the dehydratase would be in agreement with ET already being enabled by binding of the ATP-bound activator to the dehydratase. ATP-hydrolysis would then be needed to regenerate the ADP-bound state of the activator whose low affinity for the dehydratase would trigger complex dissociation allowing the cycle of reduction of the activator and ATP-

dx.doi.org/10.1021/bi300571z | *Biochemistry* 2012, 51, 6609−6622

induced complex formation between activator and dehydratase to start again.

The crystallographic analysis of Act_{Cd} presented here gives new insights into the activation mechanism of 2-hydroxyacyl-CoA dehydratases, and further work is necessary to define binding equilibria and ET rates to unravel the contributions of conformational changes and desolvation in the ATP-driven reaction of this unique class of activators.

■ ASSOCIATED CONTENT

Supporting Information

Topological scheme of an Act^{ADP} monomer; binding modes of ADP and ADPNP; structural changes upon nucleotide exchange; and superimposition of the nucleotide binding sites of Act^{ADP} and Act^{ADPNP}. This material is available free of charge via the Internet at http://pubs.acs.org.

■ AUTHOR INFORMATION

Corresponding Author

*Institut für Biologie, Strukturbiologie/Biochemie, Humboldt-Universität zu Berlin, Unter den Linden 6, D-10099 Berlin. Phone: ++49-30-2093-6369. Fax: ++49-30-2093-6447. E-mail: holger.dobbek@biologie.hu-berlin.de.

Present Address

⊥Lehrstuhl Biopolymere and Forschungszentrum für Biomakromoleküle, Universität Bayreuth, D-95440 Bayreuth, Germany.

Author Contributions

The manuscript was written through the contributions of all authors. All authors have given their approval of the final version of the manuscript.

Funding

S.K. received a stipend from the Fonds der Chemischen Industrie and was a member of ENB Graduate School on "Lead Structures of Cell Function". H.D. acknowledges the Deutsche Forschungsgemeinschaft for funding of the project (DFG-DO 785/4-1) and his position (DO 785/3-1 and Cluster of Excellence "Unifying Concepts in Catalysis−UniCat"). W.B. was funded by the Max-Planck-Society and the Fonds der Chemischen Industrie.

Notes

The authors declare no competing financial interest.

■ ACKNOWLEDGMENTS

We thank Dr. Jihoe Kim (Philipps University Marburg, Germany; present address, School of Biotechnology, Yeungnam University, Gyeongsan 712-749, South Korea) for providing the plasmids and sharing his experience on the production and purification of the activator and the dehydratase. We further thank the staff at the BESSY beamlines 14.1 and 14.2 in Berlin, Germany, for help in data collection.

■ ABBREVIATIONS USED

ADP, adenosine-5′-diphosphate; ADPNP, adenosine-5′-(β,γ-imido)-triphosphate; ATP, adenosine-5′-triphosphate; Act_{Af}, activator of 2-hydroxyglutaryl-CoA dehydratase from *Acidaminococcus fermentans*; Act_{Af}^{ADP}, Act_{Af} with bound ADP; Act_{Cd}, activator of 2-hydroxyisocaproyl-CoA dehydratase from *Clostridium difficile*; Act_{Cd}^{ADP}, Act_{Cd} with bound ADP; Act_{Cd}^{ADPNP}, Act_{Cd} with bound ADPNP; Act_{Cd}^{empty}, Act_{Cd} without nucleotide; *A. fermentans*, *Acidaminococcus fermentans*; *C. difficile*, *Clostridium difficile*; DTB, D-desthiobiotin; DTT, dithiothreitol; *E. coli*, *Escherichia coli*; MOPS, 3-(*N*-morpholino)propanesulfonic acid; MWCO, molecular weight cutoff; PDB, protein data bank

■ REFERENCES

(1) Igarashi, R. Y., and Seefeldt, L. C. (2003) Nitrogen fixation: the mechanism of the Mo-dependent nitrogenase. *Crit. Rev. Biochem. Mol. Biol. 38*, 351−384.

(2) Rees, D. C., and Howard, J. B. (2000) Nitrogenase: standing at the crossroads. *Curr. Opin. Chem. Biol. 4*, 559−566.

(3) Howard, J. B., and Rees, D. C. (1994) Nitrogenase: a nucleotide-dependent molecular switch. *Annu. Rev. Biochem. 63*, 235−264.

(4) Burgess, B. K., and Lowe, D. J. (1996) Mechanism of molybdenum nitrogenase. *Chem. Rev. 96*, 2983−3012.

(5) Nomata, J., Swem, L. R., Bauer, C. E., and Fujita, Y. (2005) Overexpression and characterization of dark-operative protochlorophyllide reductase from *Rhodobacter capsulatus*. *Biochim. Biophys. Acta 1708*, 229−237.

(6) Bröcker, M. J., Schomburg, S., Heinz, D. W., Jahn, D., Schubert, W. D., and Moser, J. (2010) Crystal structure of the nitrogenase-like dark operative protochlorophyllide oxidoreductase catalytic complex $(ChlN/ChlB)_2$. *J. Biol. Chem. 285*, 27336−27345.

(7) Muraki, N., Nomata, J., Ebata, K., Mizoguchi, T., Shiba, T., Tamiaki, H., Kurisu, G., and Fujita, Y. (2010) X-ray crystal structure of the light-independent protochlorophyllide reductase. *Nature 465*, 110−114.

(8) Ferguson, T., Soares, J. A., Lienard, T., Gottschalk, G., and Krzycki, J. A. (2009) RamA, a protein required for reductive activation of corrinoid-dependent methylamine methyltransferase reactions in methanogenic archaea. *J. Biol. Chem. 284*, 2285−2295.

(9) Schilhabel, A., Studenik, S., Vodisch, M., Kreher, S., Schlott, B., Pierik, A. J., and Diekert, G. (2009) The ether-cleaving methyltransferase system of the strict anaerobe *Acetobacterium dehalogenans*: analysis and expression of the encoding genes. *J. Bacteriol. 191*, 588−599.

(10) Siebert, A., Schubert, T., Engelmann, T., Studenik, S., and Diekert, G. (2005) Veratrol-O-demethylase of *Acetobacterium dehalogenans*: ATP-dependent reduction of the corrinoid protein. *Arch. Microbiol. 183*, 378−384.

(11) Hennig, S. E., Jeoung, J. H., Goetzl, S., and Dobbek, H. (2012) Redox-dependent complex formation by an ATP-dependent activator of the corrinoid/iron-sulfur protein. *Proc. Natl. Acad. Sci. U.S.A. 109*, 5235−5240.

(12) Kim, J., Hetzel, M., Boiangiu, C. D., and Buckel, W. (2004) Dehydration of (*R*)-2-hydroxyacyl-CoA to enoyl-CoA in the fermentation of alpha-amino acids by anaerobic bacteria. *FEMS Microbiol. Rev. 28*, 455−468.

(13) Buckel, W. (2009) Radical and electron recycling in catalysis. *Angew Chem Int Ed 48*, 6779−6787.

(14) Buckel, W., and Golding, B. T. (2006) Radical enzymes in anaerobes. *Annu. Rev. Microbiol. 60*, 27−49.

(15) Buckel, W., Zhang, J., Friedrich, P., Parthasarathy, A., Li, H., Djurdjevic, I., Dobbek, H., and Martins, B. M. (2011) Enzyme catalyzed radical dehydrations of hydroxy acids. *Biochim. Biophys. Acta*, DOI: 10.1016/j.bbapap.2011.11.009.

(16) Boll, M., Fuchs, G., and Heider, J. (2002) Anaerobic oxidation of aromatic compounds and hydrocarbons. *Curr. Opin. Chem. Biol. 6*, 604−611.

(17) Jang, S. B., Seefeldt, L. C., and Peters, J. W. (2000) Insights into nucleotide signal transduction in nitrogenase: structure of an iron protein with MgADP bound. *Biochemistry 39*, 14745−14752.

(18) Georgiadis, M. M., Komiya, H., Chakrabarti, P., Woo, D., Kornuc, J. J., and Rees, D. C. (1992) Crystallographic structure of the nitrogenase iron protein from *Azotobacter vinelandii*. *Science 257*, 1653−1659.

(19) Tezcan, F. A., Kaiser, J. T., Mustafi, D., Walton, M. Y., Howard, J. B., and Rees, D. C. (2005) Nitrogenase complexes: multiple docking sites for a nucleotide switch protein. *Science 309*, 1377−1380.

(20) Schindelin, H., Kisker, C., Schlessman, J. L., Howard, J. B., and Rees, D. C. (1997) Structure of ADP·AlF_4^--stabilized nitrogenase complex and its implications for signal transduction. *Nature 387*, 370−376.
(21) Kabsch, W., and Holmes, K. C. (1995) The actin fold. *FASEB J. 9*, 167−174.
(22) Hurley, J. H. (1996) The sugar kinase/heat shock protein 70/actin superfamily: implications of conserved structure for mechanism. *Annu. Rev. Biophys. Biomol. Struct. 25*, 137−162.
(23) Flaherty, K. M., McKay, D. B., Kabsch, W., and Holmes, K. C. (1991) Similarity of the three-dimensional structures of actin and the ATPase fragment of a 70-kDa heat shock cognate protein. *Proc. Natl. Acad. Sci. U.S.A. 88*, 5041−5045.
(24) Buss, K. A., Cooper, D. R., Ingram-Smith, C., Ferry, J. G., Sanders, D. A., and Hasson, M. S. (2001) Urkinase: structure of acetate kinase, a member of the ASKHA superfamily of phosphotransferases. *J. Bacteriol. 183*, 680−686.
(25) Bork, P., Sander, C., and Valencia, A. (1992) An ATPase domain common to prokaryotic cell cycle proteins, sugar kinases, actin, and hsp70 heat shock proteins. *Proc. Natl. Acad. Sci. U.S.A. 89*, 7290−7294.
(26) Locher, K. P., Hans, M., Yeh, A. P., Schmid, B., Buckel, W., and Rees, D. C. (2001) Crystal structure of the *Acidaminococcus fermentans* 2-hydroxyglutaryl-CoA dehydratase component A. *J. Mol. Biol. 307*, 297−308.
(27) Kim, J., Pierik, A. J., and Buckel, W. (2010) A complex of 2-hydroxyisocaproyl-coenzyme A dehydratase and its activator from *Clostridium difficile* stabilized by aluminium tetrafluoride-adenosine diphosphate. *ChemPhysChem 11*, 1307−1312.
(28) Kim, J., Darley, D., and Buckel, W. (2005) 2-Hydroxyisocaproyl-CoA dehydratase and its activator from *Clostridium difficile*. *FEBS J. 272*, 550−561.
(29) Hans, M., Bill, E., Cirpus, I., Pierik, A. J., Hetzel, M., Alber, D., and Buckel, W. (2002) Adenosine triphosphate-induced electron transfer in 2-hydroxyglutaryl-CoA dehydratase from *Acidaminococcus fermentans*. *Biochemistry 41*, 5873−5882.
(30) Hans, M., Buckel, W., and Bill, E. (2000) The iron-sulfur clusters in 2-hydroxyglutaryl-CoA dehydratase from *Acidaminococcus fermentans*. Biochemical and spectroscopic investigations. *Eur. J. Biochem. 267*, 7082−7093.
(31) Kim, J., Lu, Y., and Buckel, W. (2007) ATP- and redox-induced conformational changes in the activator of the radical enzyme 2-hydroxyisocaproyl-CoA dehydratase. *C. R. Chim. 10*, 742−747.
(32) Hans, M., Buckel, W., and Bill, E. (2008) Spectroscopic evidence for an all-ferrous $[4Fe\text{-}4S]^0$ cluster in the superreduced activator of 2-hydroxyglutaryl-CoA dehydratase from *Acidaminococcus fermentans*. *J. Biol. Inorg. Chem. 13*, 563−574.
(33) Kim, J., Darley, D. J., Buckel, W., and Pierik, A. J. (2008) An allylic ketyl radical intermediate in clostridial amino-acid fermentation. *Nature 452*, 239−242.
(34) Knauer, S. H., Buckel, W., and Dobbek, H. (2011) Structural basis for reductive radical formation and electron recycling in (*R*)-2-hydroxyisocaproyl-CoA dehydratase. *J. Am. Chem. Soc. 133*, 4342−4347.
(35) Hans, M., and Buckel, W. (2000) Purification of recombinant component A of 2-hydroxyglutaryl-CoA dehydratase from *Acidaminococcus fermentans* using Strep-Tactin affinity-chromatography. *Biotech. Int. 12*.
(36) Yount, R. G., Babcock, D., Ballantyne, W., and Ojala, D. (1971) Adenylyl imidodiphosphate, an adenosine triphosphate analog containing a P–N–P linkage. *Biochemistry 10*, 2484−2489.
(37) Kabsch, W. (1993) Automatic processing of rotation diffraction data from crystals of initially unknown symmetry and cell constants. *J. Appl. Crystallogr. 26*, 795−800.
(38) McCoy, A. J., Grosse-Kunstleve, R. W., Adams, P. D., Winn, M. D., Storoni, L. C., and Read, R. J. (2007) Phaser crystallographic software. *J. Appl. Crystallogr. 40*, 658−674.
(39) Terwilliger, T. C. (2003) Automated main-chain model building by template matching and iterative fragment extension. *Acta Crystallogr., Sect. D 59*, 38−44.
(40) Emsley, P., Lohkamp, B., Scott, W., and Cowtan, K. (2010) Features and development of COOT. *Acta Crystallogr., Sect. D 66*, 486−501.
(41) Adams, P. D., Afonine, P. V., Bunkoczi, G., Chen, V. B., Davis, I. W., Echols, N., Headd, J. J., Hung, L. W., Kapral, G. J., Grosse-Kunstleve, R. W., McCoy, A. J., Moriarty, N. W., Oeffner, R., Read, R. J., Richardson, D. C., Richardson, J. S., Terwilliger, T. C., and Zwart, P. H. (2010) PHENIX: a comprehensive Python-based system for macromolecular structure solution. *Acta Crystallogr., D 66*, 213−221.
(42) Schrödinger, L. (2010) *The PyMOL Molecular Graphics System*, version 1.2, DeLano Scientific, Palo Alto, CA.
(43) Kleywegt, G. J., and Jones, T. A. (1997) Detecting folding motifs and similarities in protein structures. *Methods Enzymol. 277*, 525−545.
(44) Ho, B. K., and Gruswitz, F. (2008) HOLLOW: generating accurate representations of channel and interior surfaces in molecular structures. *BMC Struct. Biol. 8*, 49.
(45) Koradi, R., Billeter, M., and Wuthrich, K. (1996) MOLMOL: a program for display and analysis of macromolecular structures. *J. Mol. Graph. 14* (51−55), 29−32.
(46) Gasteiger, E., Gattiker, A., Hoogland, C., Ivanyi, I., Appel, R. D., and Bairoch, A. (2003) ExPASy: The proteomics server for in-depth protein knowledge and analysis. *Nucleic Acids Res. 31*, 3784−3788.
(47) Glusker, J. P. (1991) Structural aspects of metal liganding to functional groups in proteins. *Adv. Protein Chem. 42*, 1−76.
(48) Harrison, C. J., Hayer-Hartl, M., Di Liberto, M., Hartl, F., and Kuriyan, J. (1997) Crystal structure of the nucleotide exchange factor GrpE bound to the ATPase domain of the molecular chaperone DnaK. *Science 276*, 431−435.
(49) Anderson, C. M., Stenkamp, R. E., McDonald, R. C., and Steitz, T. A. (1978) A refined model of the sugar binding site of yeast hexokinase B. *J. Mol. Biol. 123*, 207−219.
(50) Anderson, C. M., McDonald, R. C., and Steitz, T. A. (1978) Sequencing a protein by x-ray crystallography. I. Interpretation of yeast hexokinase B at 2.5 A resolution by model building. *J. Mol. Biol. 123*, 1−13.
(51) Robinson, R. C., Turbedsky, K., Kaiser, D. A., Marchand, J. B., Higgs, H. N., Choe, S., and Pollard, T. D. (2001) Crystal structure of Arp2/3 complex. *Science 294*, 1679−1684.
(52) Boehr, D. D., and Wright, P. E. (2008) Biochemistry. How do proteins interact? *Science 320*, 1429−1430.
(53) Schuler, H. (2001) ATPase activity and conformational changes in the regulation of actin. *Biochim. Biophys. Acta 1549*, 137−147.
(54) Wilbanks, S. M., Chen, L., Tsuruta, H., Hodgson, K. O., and McKay, D. B. (1995) Solution small-angle X-ray scattering study of the molecular chaperone Hsc70 and its subfragments. *Biochemistry 34*, 12095−12106.
(55) Flaherty, K. M., Wilbanks, S. M., DeLuca-Flaherty, C., and McKay, D. B. (1994) Structural basis of the 70-kilodalton heat shock cognate protein ATP hydrolytic activity. II. Structure of the active site with ADP or ATP bound to wild type and mutant ATPase fragment. *J. Biol. Chem. 269*, 12899−12907.
(56) Page, C. C., Moser, C. C., Chen, X., and Dutton, P. L. (1999) Natural engineering principles of electron tunnelling in biological oxidation-reduction. *Nature 402*, 47−52.
(57) Dey, A., Jenney, F. E., Jr., Adams, M. W., Babini, E., Takahashi, Y., Fukuyama, K., Hodgson, K. O., Hedman, B., and Solomon, E. I. (2007) Solvent tuning of electrochemical potentials in the active sites of HiPIP versus ferredoxin. *Science 318*, 1464−1468.
(58) Noodleman, L., Lovell, T., Liu, T., Himo, F., and Torres, R. A. (2002) Insights into properties and energetics of iron-sulfur proteins from simple clusters to nitrogenase. *Curr. Opin. Chem. Biol. 6*, 259−273.
(59) Thamer, W., Cirpus, I., Hans, M., Pierik, A. J., Selmer, T., Bill, E., Linder, D., and Buckel, W. (2003) A two [4Fe-4S]-cluster-containing ferredoxin as an alternative electron donor for 2-

hydroxyglutaryl-CoA dehydratase from *Acidaminococcus fermentans*. *Arch. Microbiol. 179*, 197−204.
(60) Thauer, R. K., Jungermann, K., and Decker, K. (1977) Energy conservation in chemotrophic anaerobic bacteria. *Bacteriol. Rev. 41*, 100−180.
(61) Dolinsky, T. J., Nielsen, J. E., McCammon, J. A., and Baker, N. A. (2004) PDB2PQR: an automated pipeline for the setup of Poisson-Boltzmann electrostatics calculations. *Nucleic Acids Res. 32*, W665−667.
(62) Dolinsky, T. J., Czodrowski, P., Li, H., Nielsen, J. E., Jensen, J. H., Klebe, G., and Baker, N. A. (2007) PDB2PQR: expanding and upgrading automated preparation of biomolecular structures for molecular simulations. *Nucleic Acids Res. 35*, W522−525.
(63) Baker, N. A., Sept, D., Joseph, S., Holst, M. J., and McCammon, J. A. (2001) Electrostatics of nanosystems: application to microtubules and the ribosome. *Proc. Natl. Acad. Sci. U.S.A. 98*, 10037−10041.